Journal Name

ARTICLE TYPE

Cite this: DOI: 10.1039/xxxxxxxxxx

Dynamics and Morphology of Solid Electrolyte Interphase (SEI)†

Fabian Single,[a,b,‡] Birger Horstmann,*[a,b,‡] and Arnulf Latz [a,b,c]

Received Date
Accepted Date

DOI: 10.1039/xxxxxxxxxx

www.rsc.org/journalname

We develop a novel theory for the continuous electrochemical formation of porous films to study the solid electrolyte interphase (SEI) on lithium ion battery anodes. Existing SEI studies model a homogeneous morphology and a single relevant transport mechanism. Our approach, in contrast, is based on two transport mechanisms and enables us to track SEI porosity in a spatially resolved way. SEI thickness evolution agrees with existing studies and is validated with experiments. This consistent approach is unprecedented in SEI modeling. We predict a non-zero SEI porosity and the dependence of morphology on transport properties. Additionally, we capture dual-layer chemistry and morphology. Analytic expressions which describe the parameter dependence of all key properties are derived and discussed.

The formation of a stable interfacial layer, the so-called solid electrolyte interphase (SEI), on graphite anodes has enabled the success of Li-ion batteries (LIBs)[1]. In these batteries, electrolyte solvent is unstable at typical working potentials[2,3]. Solvent reduction products form a thin layer separating anode and electrolyte, the so-called solid electrolyte interphase (SEI). A well-formed SEI significantly slows down further electrolyte reduction, resulting in the excellent cycling stability of LIBs. However, electrolyte reduction and SEI formation are never fully suppressed and remain the major cause for long-term capacity fade[4–6].

This critical role has led to numerous experimental and theoretical studies of the SEI. Experimental results are summarized in review articles and systematic studies[7–14]. Recently, isotope tracer experiments demonstrated the potential-dependent dual-layer structure of the SEI[15–17]. It is generally accepted that the SEI consists of a dense inner layer close to the electrode and a porous outer layer. Several long-term measurements find that capacity fade scales with the square root of time[18–20], a strong indication that SEI formation is a transport limited process. This observation is explored in numerous theoretical studies which use a single rate determining transport mechanism to describe SEI growth. SEI formation controlled by solvent diffusion is assumed by Pinson and Bazant[21] and Ploehn[4], whereas electron conduction mechanisms are considered by Peled[22], Christensen[23], Li[24] and Lin[25]. Most studies describe the evolution of a homogeneous SEI layer with a sharp interface and do not attempt to account for spatial heterogeneity. Only a few models consider a spa-

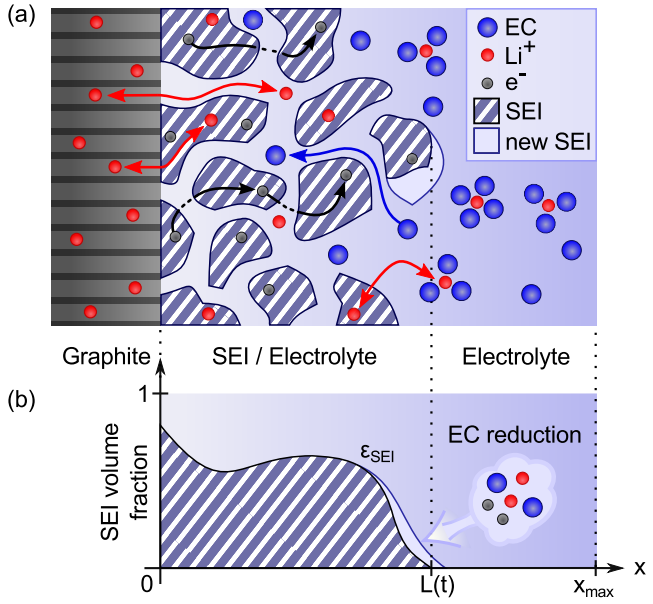

Fig. 1 (a) Cross section through graphite electrode, SEI and electrolyte depicting all relevant species: solvent molecules EC, lithium ions Li^+, and electrons e^-. EC and e^- move in opposite directions (single headed arrows). (b) Profile of the averaged SEI volume fraction along the axis perpendicular to the electrode surface.

* Corresponding Author: *birger.horstmann@dlr.de*
[a] *German Aerospace Center (DLR), Institute of Engineering Thermodynamics, Pfaffenwaldring 38-40, 70569 Stuttgart, Germany*
[b] *Helmholtz Institute Ulm (HIU), Helmholtzstraße 11, 89081 Ulm, Germany*
[c] *Ulm University, Institute of Electrochemistry, Albert-Einstein-Allee 47, 89069 Ulm, Germany*
† Electronic Supplementary Information (ESI) available: [Enter DOI].
‡These authors contributed equally to this work.

tially resolved interface with the electrolyte or an inhomogeneous SEI[26,27].

Despite substantial differences in the chosen rate-limiting transport mechanism, all available models predict SEI thickness evolution in agreement with experiments. Thus, they remain inconclusive with respect to the rate limiting process. Conclusions require further observable predictions with respect to SEI morphology, e.g., porosity and dual-layer structure. For this reason, we develop a theory for the growth of a porous and inhomogeneous layer. Our model studies the dynamics of film porosity in one dimension, perpendicular to the substrate surface. This is possible because the transport of all film precursors within the porous structure is taken into account.

In this work we formulate and parameterize our model specifically to describe SEI evolution, as depicted in Figure 1. We apply the popular porous electrode theory to the nano-porous SEI. To this aim SEI composition and morphology are averaged in slabs parallel to the anode surface. Thus film growth is modeled along a single coordinate x, see Figure 1(b). Within the simulation domain we trace the transport of all species involved in SEI formation. Here we assume electron conduction in the SEI material[23]. In the electrolyte, solvent molecules diffuse towards the electrode[21]. The electrochemical potential of lithium ions is assumed to be constant at all times and does not result in inhomogeneous reaction rates. This assumption is justified because lithium ion transport in the SEI[28] is very fast compared to SEI growth, i.e., SEI growth consumes small amounts of lithium and transport quickly restores local equilibrium. SEI is formed when reactions between charge moving away from the electrode and solvent moving towards the electrode occur. In summary, we model diffusion of solvent and conduction of electrons. Therefore, electronic conductivity and solvent diffusivity are key parameters.

The bulk electrolyte phase is a binary mixture of ethylene carbonate (EC) with co-solvent dimethyl carbonate (DMC), i.e., EC:DMC 3:7. As we focus on morphology, SEI chemistry is further simplified by neglecting the salt anion. Because ionic species are neglected, double layer effects[29] cannot be included in our model. Only a single representative reduction reaction per solvent species is considered

$$2\mathrm{EC} + 2\mathrm{Li}^+ + 2\mathrm{e}^- \rightarrow \mathrm{Li_2EDC}\downarrow + \mathrm{R_{EC}}\uparrow, \tag{1a}$$

$$\mathrm{DMC} + \mathrm{Li}^+ + \mathrm{e}^- \rightarrow \mathrm{LiMC}\downarrow + \mathrm{R_{DMC}}\uparrow. \tag{1b}$$

We choose lithium ethylene dicarbonate (Li_2EDC) as a product of EC reduction[30,31] and lithium methyl carbonate (LiMC) from DMC reduction[32]. Gaseous reaction byproducts R_i are neglected. Hereinafter, indices i refer to $i = \mathrm{EC}, \mathrm{DMC}$ or $i = \mathrm{Li_2EDC}, \mathrm{LiMC}$ depending on the phase (electrolyte/SEI) of the corresponding variable/parameter.

The production rate $\dot{s}_i$ of each SEI compound drives the evolution of the volume fraction ε_i

$$\frac{\partial \varepsilon_i}{\partial t} = \bar{V}_i^{\mathrm{S}} \dot{s}_i, \tag{2}$$

where $\bar{V}_i^{S}$ is the molar volume of SEI compound i. This means a solvation/precipitation mechanism[33] is not considered. Solvent molecules move through the electrolyte phase via diffusion and convection. The evolution of solvent concentration c_i is coupled to sink terms from SEI formation with mass balance equations

$$\frac{\partial \varepsilon c_i}{\partial t} = -\operatorname{div}\left(j_{\mathrm{D},i} + j_{\mathrm{C},i}\right) - \nu_i \dot{s}_i, \tag{3}$$

where $\varepsilon = 1 - \sum \varepsilon_i$ is the local porosity and $\nu_{\mathrm{EC}} = 2$ / $\nu_{\mathrm{DMC}} = 1$ are stoichiometric coefficients. According to Fick's law, diffusion is driven by concentration gradients $j_{\mathrm{D},i} = -D_i \operatorname{grad} c_i$. Convection is determined by the velocity v of the electrolyte $j_{\mathrm{C},i} = c_i v$. By treating the mixture as an incompressible fluid, we use the volume constraint $\sum \bar{V}_i^{\mathrm{E}} c_i = 1$ to eliminate the co-solvent concentration[34]. Because v is the center-of-mass velocity, we require $D_{\mathrm{DMC}} = D_{\mathrm{EC}} \cdot M_{\mathrm{EC}} V_{\mathrm{DMC}} / (M_{\mathrm{DMC}} V_{\mathrm{EC}})$ with molar masses M_i. Volume constraint and mass balance equations (3) together determine the convective velocity[35,36]

$$\begin{aligned} \operatorname{div} v = &\sum \left(\bar{V}_i^{\mathrm{S}} - \nu_i \bar{V}_i^{\mathrm{E}}\right) \dot{s}_i \\ &+ \bar{V}_{\mathrm{EC}}^{\mathrm{E}} \operatorname{div}\left(D_{\mathrm{EC}} - D_{\mathrm{DMC}}\right) \operatorname{grad} c_{\mathrm{EC}}. \end{aligned} \tag{4}$$

Conservation of "electronic charges" is ensured via

$$0 = -\operatorname{div} j_{\mathrm{E}} + F\left(2\dot{s}_{\mathrm{Li_2EDC}} + \dot{s}_{\mathrm{LiMC}}\right), \tag{5}$$

where the electron current depends on the electric potential Φ through Ohm's law $j_{\mathrm{E}} = -\kappa \operatorname{grad} \Phi$. We solve equations (2)-(5) for the spatially-resolved dynamics of $\varepsilon_{\mathrm{Li_2EDC}}, \varepsilon_{\mathrm{LiMC}}, c_{\mathrm{EC}}, \Phi$, and v within the simulation domain $[0, x_{\max}]$.

Volume-averaged transport parameters D_i and κ contain the effects of porosity and tortuosity. The Bruggeman ansatz relates them to their bulk values using the local porosity and SEI volume fraction $\varepsilon_{\mathrm{SEI}} = 1 - \varepsilon$,

$$D_i = \varepsilon^{\beta} D_i^0 \quad \text{and} \quad \kappa = \varepsilon_{\mathrm{SEI}}^{1.5} \kappa^0, \tag{6}$$

where 1.5 is the standard Bruggeman coefficient for conduction[37] in porous media. For simplicity, we choose the same electronic bulk conductivity κ^0 for all SEI compounds. We use large values of $\beta \sim 20$ in our model, representing the difficulty of electrolyte transport in nano-pores.

The compound production rates $\dot{s}_i = A_i \Gamma \dot{r}_i$ depend on specific surface areas A_i, surface site density Γ, and reaction rates $\dot{r}_i$. The latter are given by a symmetric Butler-Volmer expression[38,39],

$$\dot{r}_i = \frac{1}{2} \frac{k_{\mathrm{B}} T}{h} \left(\frac{c_i}{c_i^0}\right)^{\frac{\nu_i}{2}} \exp\left(\frac{-E_A}{k_{\mathrm{B}} T}\right) \sinh \frac{F \eta_i}{RT}, \tag{7}$$

where solvent reduction is driven by the overpotentials

$$\eta_i = -\left(\Phi - \Phi_i^0\right) + \frac{RT}{F} \ln\left(\frac{c_i}{c_i^0}\right). \tag{8}$$

Reduction reactions are in equilibrium when potential and concentrations are Φ_i^0 and c_i^0, respectively. The activation barrier of the reaction E_{A} is twice the desolvation energy of Li^+ in EC[40,41]. We represent the irreversibility of these reactions by setting $\dot{r}_i = 0$ for negative η, i.e., we disregard the oxidation (SEI components

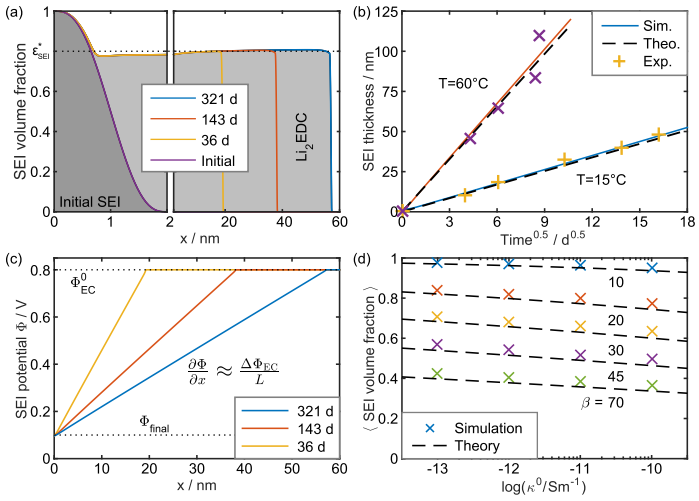

Fig. 2 Results with inert co-solvent. (a) Temporal evolution of the SEI volume fraction $\varepsilon_{Li_2EDC} + \varepsilon_{init}$ ($\kappa^0 = 0.3\,\mathrm{pS\,m^{-1}}$, $\beta = 25$, $T = 15^\circ\mathrm{C}$). (b) SEI thickness evolution from experiment [19,21] (dots), simulation (dashed) and eq (11) (lines). (c) SEI potential distribution at different stages of SEI evolution, corresponding to (a) . (d) Influence of β and κ^0 on ε^*_{SEI}, analytic results from eq (13) (dashed lines) compared to simulation results (dots). The values were obtained by averaging $\varepsilon_{SEI}(x)$ between 2 nm and 55 nm after simulating the growth of a 60 nm thick layer.

are oxidized at $\Phi \approx 3.25\,\mathrm{V}$ [42]).

A continuous expression is used for the specific surface area. As derived in the supplementary material‡,

$$A_i = \frac{6}{a_0}\varepsilon\left(\tilde{\varepsilon}_i + \frac{a_0^2}{6}\frac{\partial^2\tilde{\varepsilon}_i}{\partial x^2}\right),\ \tilde{\varepsilon}_i = \varepsilon_i + \varepsilon_{init}. \tag{9}$$

This smoothes the porosity profile and distributes growth such that the SEI front has finite thickness. Additionally it enables propagation of SEI into the electrolyte as well as numerical convergence.

Simulation details, such as initialization, boundary conditions and parameters are discussed in the supplementary material‡.

Inert Co-Solvent. We start our discussion with the special case of an inert co-solvent, i.e., we disable co-solvent reduction ($i_{DMC} = 0$) and study the growth of an SEI with homogeneous chemistry. A typical evolution of SEI volume fraction is depicted in Figure 2(a). We find that growth is concentrated at the SEI front whose spatial width lies in the order of a_0. Thus, electron conduction through the SEI becomes the rate limiting process in our model. The porosity inside the SEI attains a nearly constant value $\varepsilon(x) \approx \varepsilon^* = 1 - \varepsilon^*_{SEI}$ which we explain below. On closer inspection we find that SEI volume fraction increases slightly with distance from electrode.

In our model the SEI thickness grows with the square root of time in agreement with experiments (see Figure 2(b)). It has been shown previously that this can be rationalized based on a single rate limiting transport process [4,21]. Therefore, we obtain SEI conductivity by fitting the simulated thickness evolution to experimental data. With capacity fade measurements of Liu et al. [19] and an estimate for the electrode surface area by Pinson et al. [21] we find $\kappa^0 = 0.3\,\mathrm{pS\,m^{-1}}$ at $T = 15^\circ\mathrm{C}$ and $\kappa^0 = 4.5\,\mathrm{pS\,m^{-1}}$ at $T = 60^\circ\mathrm{C}$ (with $\beta = 25$). These low electron conductivities ensure good passivation and are below the ones for artificial SEIs [43]. The microscopic mechanism underlying this conductivity is still under investigation. Besides conventional conduction, successive electron tunneling [25] or neutral lithium interstitial diffusion [28] are potential mechanisms.

In Figure 2(c) we show that the potential increases linearly from the value Φ_{final} at the electrode to Φ^0_{EC} at the SEI front. The linearity demonstrates that crystallization inside the SEI is negligible. A potential drop over the SEI interface is absent because the formation reaction is fast. For a constant porosity ε^* and a linear potential $\Phi(x,t)$ we can approximate the electric current through the bulk SEI phase and calculate the thickness evolution

$$\frac{\partial L}{\partial t} = -\frac{j_E}{2F}\frac{\bar{V}^S_{Li_2EDC}}{\varepsilon^*_{SEI}} \approx \frac{\varepsilon^{*1/2}_{SEI}\kappa^0\Delta\Phi_{EC}\bar{V}^S_{Li_2EDC}}{2F}\frac{1}{L}, \tag{10}$$

$$\Rightarrow L(t) = \sqrt{\frac{\varepsilon^{*1/2}_{SEI}\kappa^0\Delta\Phi_{EC}\bar{V}^S_{Li_2EDC}}{F}}\cdot\sqrt{t}. \tag{11}$$

We note that SEI growth is essentially governed by the potential difference $\Delta\Phi_{EC} = \Phi^0_{EC} - \Phi_{final}$. Figure 2(b) proofs the excellent agreement between experiment, simulation and eq (11).

We derive an expression for the nearly constant SEI porosity ε^* in this SEI layer. Our approach traces the SEI formation rate in the frame co-moving with the SEI front

$$\frac{\mathrm{d}\varepsilon(L,t)}{\mathrm{d}t} = \frac{\partial\varepsilon}{\partial t} + \frac{\partial\varepsilon}{\partial L}\frac{\partial L}{\partial t}. \tag{12}$$

With few assumptions, i.e., no convection and infinitely fast reactions, we find that $\varepsilon(L,t)$ in eq (12) has a stationary solution ε^*. This means that in time, the porosity in the co-moving frame tends towards this stable value. An implicit expression for ε^* can be derived from eq (12)

$$\kappa(\varepsilon^*) = D(\varepsilon^*)\frac{F^2 c^0_{EC}}{RT}\left(\frac{1}{2} + \beta\frac{1-\varepsilon^*}{\varepsilon^*}\right). \tag{13}$$

Our simulations show that eq (13) gives an excellent estimate for the dependence of the porosity ε^* on the transport parameters. Very good quantitative agreement is observed for small EC concentrations, see Figure 2(d). It can be seen that β is the parameter with the highest influence on film porosity. The film porosity is a direct consequence of an interplay between solvent species crossing the moving SEI front and SEI expansion. As the film becomes denser, solvent transport into the film is slowed down. Eventually further growth is distributed such that the film expands and the density no longer increases. As shown in Figure 2(d), large values of β are needed to see this effect. At $\beta = 10$, film density is nearly one, $\varepsilon^*_{SEI} \approx 0.98$.

Reactive Co-Solvent. In the following, we discuss simulations with simultaneous solvent and co-solvent reduction. Figure 3(a) depicts the corresponding evolution of both SEI volume fractions. Next to the electrode, LiMC grows "on top" of the Li_2EDC phase. This forms a dense inner layer with $\varepsilon_{SEI}(x) \approx 1$ while the porous outer layer with $\varepsilon_{SEI}(x) \approx \varepsilon^*_{SEI}$ remains. At $\Phi^0_{EC} = 0.8$ V EC starts to create a SEI layer with pores containing DMC as shown in Fig-

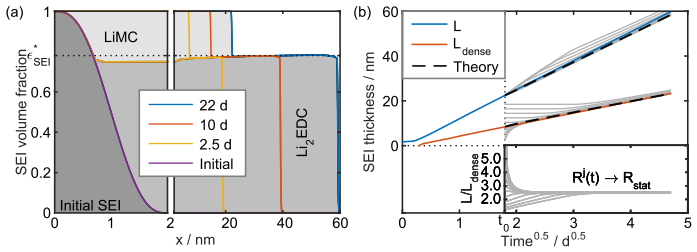

Fig. 3 (a) Temporal evolution of the SEI volume fraction with two reduction reactions ($\kappa^0 = 4.5\,\mathrm{pS\,m^{-1}}$, $\beta = 25$, $T = 60^\circ\mathrm{C}$). (b) Same simulation, evolution of total and dense SEI layer thickness (lines) compared to numerical solutions of the analytical approximation eq (14a) (dashed). Additional numerical solutions with different $L^j_{\mathrm{dense}}(t_0)$ $(j = 1,\ldots,10)$ indicate, how SEI growth continues when $R \neq R_{\mathrm{stat}}$ (thin grey lines). The inset in the bottom-right corner shows the corresponding evolution of $R^j = L^j/L^j_{\mathrm{dense}}$.

ure 2(a). When the potential drops below $\Phi^0_{\mathrm{DMC}} = 0.3$ V, DMC is reduced to form LiMC. Consequently the dense layer appears near the electrode where the potential is lower. This dual-layer structure agrees with experimental observations[17]. Similar to co-solvent reduction, it would emerge from a conversion of the primary SEI compound at low potentials[44]. Because the reduction potential of EC is higher than the one of the co-solvent (see Borodin et al.[45,46]), SEI mostly consists of EC reduction products, as recently validated by Grey et al.[47].

We compare the evolution of total SEI thickness L and the thickness of the dense layer L_{dense} in Figure 3(b). Both quickly attain their asymptotic values corresponding to square root like growth. Analogous to eq (11), SEI growth is driven by potential differences

$$\frac{\partial L}{\partial t} = \frac{\bar{V}^{\mathrm{S}}_{\mathrm{Li_2EDC}}\kappa^0}{2\varepsilon^*_{\mathrm{SEI}}F}\frac{\varepsilon^{*3/2}_{\mathrm{SEI}}\Delta\Phi_{\mathrm{diff}}}{L - L_{\mathrm{den.}}}, \tag{14a}$$

$$\frac{\partial L_{\mathrm{den.}}}{\partial t} = \frac{\bar{V}^{\mathrm{S}}_{\mathrm{LiMC}}\kappa^0}{2\varepsilon^* F}\left(\frac{\Delta\Phi_{\mathrm{DMC}}}{L_{\mathrm{den.}}} - \frac{\varepsilon^{*3/2}_{\mathrm{SEI}}\Delta\Phi_{\mathrm{diff}}}{L - L_{\mathrm{den.}}}\right) \tag{14b}$$

with $\Delta\Phi_{\mathrm{diff}} = \Phi^0_{\mathrm{EC}} - \Phi^0_{\mathrm{DMC}}$. For simple notation, this equation holds for reversible reactions only. Numerical solutions for a slightly modified system, viable for irreversible reactions are shown in Figure 3(b). Both systems are identical, when $\partial_t L_{\mathrm{dense}}$ as written in eq (14b) is positive. The inset in Figure 3(b) shows that independent of initialization, the ratio $R = L/L_{\mathrm{dense}}$ quickly approaches a stationary value R_{stat} stated as quadratic expression

$$\begin{aligned}\frac{\Delta\Phi_{\mathrm{DMC}}}{\Delta\Phi_{\mathrm{diff}}}R^2_{\mathrm{stat}} - \left(\frac{\Delta\Phi_{\mathrm{DMC}}}{\Delta\Phi_{\mathrm{diff}}} + \varepsilon^{*3/2}_{\mathrm{SEI}}\right)R_{\mathrm{stat}} \\ = \varepsilon^*\sqrt{\varepsilon^*_{\mathrm{SEI}}}\frac{\bar{V}^{\mathrm{S}}_{\mathrm{Li_2EDC}}}{\bar{V}^{\mathrm{S}}_{\mathrm{LiMC}}}.\end{aligned} \tag{15}$$

Eq (15) relates system parameters to the ratio of total SEI thickness over the thickness of the dense layer. We suggest to design the SEI and increase the ratio R_{stat} by adjusting electrolyte composition. This would increase its overall elasticity and allow it to withstand volume changes of electrode particles[48,49]. It allows the validation of our model and/or an estimate of unknown reaction properties from observable SEI properties.

In conclusion, we formulate a novel SEI growth model which extends the common approach of transport limited models. Our theory predicts long-term SEI thickness evolution in agreement with previous models and experiments, i.e., we retain square-root like growth. Additionally, we present the first continuum model which predicts properties of SEI structure. The competition between two counter-moving transport mechanisms, i.e., electron conduction and solvent diffusion, leads to a non-zero SEI porosity. This is a novel insight into porous film growth beyond the standard case of SEI formation on graphite anodes. Two distinct formation reactions result in a dual-layer structure with a dense inner layer and a porous outer layer. Porosity is constant within each layer. We can understand these properties and derive formulas for SEI thickness, SEI porosity, and thickness of the dense layer. Long-term in-situ experiments, similar to[50,51], should allow to test and refine our predictions. We hope that this kind of modeling can be extended to lithium transport through the SEI and the effect of electrochemical double layers. This would allow better understanding of SEI impedance spectra.

This work was supported by the German Federal Ministry of Education and Research (BMBF) in the project Li-EcoSafe (03X4636A). The authors would like to thank Erkmen Karaca for fruitful discussions. Further support was provided, by the bwHPC initiative and the bwHPC-C5 project through associated compute services of the JUSTUS HPC facility at the University of Ulm.

References

1 J. Vetter, P. Novák, M. R. Wagner, C. Veit, K.-C. Möller, J. O. Besenhard, M. Winter, M. Wohlfahrt-Mehrens, C. Vogler and A. Hammouche, *Journal of Power Sources*, 2005, **147**, 269–281.
2 S. Kang, M. H. Park, H. Lee and Y. K. Han, *Electrochemistry Communications*, 2012, **23**, 83–86.
3 M. Metzger, C. Marino, J. Sicklinger, D. Haering and H. A. Gasteiger, *Journal of the Electrochemical Society*, 2015, **162**, A1123–A1134.
4 H. J. Ploehn, P. Ramadass and R. E. White, *Journal of The Electrochemical Society*, 2004, **151**, A456.
5 J. Vetter, P. Novák, M. R. Wagner, C. Veit, K. C. Möller, J. O. Besenhard, M. Winter, M. Wohlfahrt-Mehrens, C. Vogler and A. Hammouche, *Journal of Power Sources*, 2005, **147**, 269–281.
6 M. Broussely, P. Biensan, F. Bonhomme, P. Blanchard, S. Herreyre, K. Nechev and R. J. Staniewicz, *Journal of Power Sources*, 2005, **146**, 90–96.
7 D. Aurbach, A. Zaban, Y. Ein-Eli, I. Weissman, O. Chusid, B. Markovsky, M. Levi, E. Levi, A. Schechter and E. Granot, *Journal of Power Sources*, 1997, **68**, 91–98.
8 D. Aurbach, B. Markovsky, I. Weissman, E. Levi and Y. Ein-Eli, *Electrochimica Acta*, 1999, **45**, 67–86.
9 D. Aurbach, *Journal of Power Sources*, 2000, **89**, 206–218.
10 S. S. Zhang, *Journal of Power Sources*, 2006, **162**, 1379–1394.
11 P. Verma, P. Maire and P. Novák, *Electrochimica Acta*, 2010, **55**, 6332–6341.
12 A. V. Agubra and J. W. Fergus, *Journal of Power Sources*, 2014, **268**, 153–162.
13 A. M. Haregewoin, E. G. Leggesse, J.-C. Jiang, F.-M. Wang, B.-J. Hwang and S. D. Lin, *Electrochimica Acta*, 2014, **136**, 274–285.
14 F. A. Soto, Y. Ma, J. M. Martinez De La Hoz, J. M. Seminario and P. B. Balbuena, *Chemistry of Materials*, 2015, **27**, 7990–8000.
15 P. Lu and S. J. Harris, *Electrochemistry Communications*, 2011, **13**, 1035–1037.
16 S. J. Harris and P. Lu, *Journal of Physical Chemistry C*, 2013, **117**, 6481–6492.
17 P. Lu, C. Li, E. W. Schneider and S. J. Harris, *Journal of Physical Chemistry C*, 2014, **118**, 896–903.
18 M. Broussely, S. Herreyre, P. Biensan, P. Kasztejna, K. Nechev and R. J. Staniewicz, *Journal of Power Sources*, 2001, **97-98**, 13–21.
19 P. Liu, J. Wang, J. Hicks-Garner, E. Sherman, S. Soukiazian, M. Verbrugge, H. Tataria, J. Musser and P. Finamore, *Journal of The Electrochemical Society*, 2010, **157**, A499.
20 A. J. Smith, J. C. Burns, X. Zhao, D. Xiong and J. R. Dahn, *Journal of The Electrochemical Society*, 2011, **158**, A447–A452.
21 M. B. Pinson and M. Z. Bazant, *Journal of the Electrochemical Society*, 2012, **160**, A243–A250.
22 E. Peled, *Journal of The Electrochemical Society*, 1979, **126**, 2047–2051.

23 J. Christensen and J. Newman, *Journal of The Electrochemical Society*, 2004, **151**, A1977.
24 D. Li, D. Danilov, Z. Zhang, H. Chen, Y. Yang and P. H. L. Notten, *Journal of the Electrochemical Society*, 2015, **162**, A858–A869.
25 Y. X. Lin, Z. Liu, K. Leung, L. Q. Chen, P. Lu and Y. Qi, *Journal of Power Sources*, 2016, **309**, 221–230.
26 J. Deng, G. J. Wagner and R. P. Muller, *Journal of the Electrochemical Society*, 2013, **160**, A487–A496.
27 P. Guan, L. Liu and X. Lin, *Journal of the Electrochemical Society*, 2015, **162**, A1798–A1808.
28 S. Shi, P. Lu, Z. Liu, Y. Qi, L. G. Hector, H. Li and S. J. Harris, *Journal of the American Chemical Society*, 2012, **134**, 15476–15487.
29 Q. Zhang, J. Pan, P. Lu, Z. Liu, M. W. Verbrugge, B. W. Sheldon, Y. T. Cheng, Y. Qi and X. Xiao, *Nano Letters*, 2016, **16**, 2011–2016.
30 G. V. Zhuang, K. Xu, H. Yang, T. R. Jow and P. N. Ross, *Journal of Physical Chemistry B*, 2005, **109**, 17567–17573.
31 K. Leung, *Chemical Physics Letters*, 2013, **568-569**, 1–8.
32 D. M. Seo, D. Chalasani, B. S. Parimalam, R. Kadam, M. Nie and B. L. Lucht, *ECS Electrochemistry Letters*, 2014, **3**, A91–A93.
33 O. Borodin and D. Bedrov, *The Journal of Physical Chemistry C*, 2014, **118**, 18362–18371.
34 B. Horstmann, T. Danner and W. G. Bessler, *Energy and Environmental Science*, 2013, **6**, 1299–1314.
35 D. Bothe and W. Dreyer, *Acta Mechanica 226*, 2015, **226**, 1757–1805.
36 S. de Groot and P. Mazur, *Non-equilibrium Thermodynamics*, Dover Publications, 1962.
37 M. Doyle, *Journal of The Electrochemical Society*, 1993, **140**, 1526.
38 A. Latz and J. Zausch, *Journal of Power Sources*, 2011, **196**, 3296–3302.
39 M. Z. Bazant, *Accounts of Chemical Research*, 2013, **46**, 1144–1160.
40 Y. Yamada, Y. Iriyama, T. Abe and Z. Ogumi, *Langmuir*, 2009, **25**, 12766–12770.
41 K. Xu, A. Von Cresce and U. Lee, *Langmuir*, 2010, **26**, 11538–11543.
42 M. Tang and J. Newman, *Journal of The Electrochemical Society*, 2012, **159**, A281.
43 J. Li, N. J. Dudney, J. Nanda and C. Liang, *ACS Applied Materials and Interfaces*, 2014, **6**, 10083–10088.
44 K. Leung, F. a. Soto, K. Hankins, P. B. Balbuena and K. L. Harrison, *The Journal of Physical Chemistry C*, 2016, **120**, 6302–6313.
45 O. Borodin, M. Olguin, C. E. Spear, K. W. Leiter and J. Knap, *Nanotechnology*, 2015, **26**, 354003.
46 O. Borodin, M. Olguin, P. Ganesh, P. R. C. Kent, J. L. Allen and W. a. Henderson, *Phys. Chem. Chem. Phys.*, 2016, **18**, 164–175.
47 A. L. Michan, M. Leskes and C. P. Grey, *Chemistry of Materials*, 2015, 385–398.
48 J. Zhang, X. Yang, R. Wang, W. Dong, W. Lu, X. Wu, X. Wang, H. Li and L. Chen, *Journal of Physical Chemistry C*, 2014, **118**, 20756–20762.
49 V. Kuznetsov, A. H. Zinn, G. Zampardi, S. Borhani-Haghighi, F. La Mantia, A. Ludwig, W. Schuhmann and E. Ventosa, *ACS Applied Materials and Interfaces*, 2015, **7**, 23554–23563.
50 G. M. Veith, M. Doucet, J. K. Baldwin, R. L. Sacci, T. M. Fears, Y. Wang and J. F. Browning, *Journal of Physical Chemistry C*, 2015, **119**, 20339–20349.
51 R. L. Sacci, J. M. Black, N. Balke, N. J. Dudney, K. L. More and R. R. Unocic, *Nano Letters*, 2015, **15**, 2011–2018.